

## A MODELLING APPROACH TO ESTIMATE BATH AND METAL HEAT TRANSFER COEFFICIENTS

Dagoberto S. Severo, Vanderlei Gusberti

PCE Engenharia S/S Ltda, Rua Caeté 162, Porto Alegre RS – Brazil – pce@pce.com.br

Keywords: Aluminum reduction, Heat transfer coefficient, Bubble driven flow, Magnetohydrodynamics, Numerical simulation

### Abstract

Heat transfer coefficients between the cell cavity and the liquids (bath and metal) are important parameters for correct thermal calculations of the electrolytic cell behavior. Traditionally, the wall heat transfer coefficients are adjusted with help of thermal measurements done in operating cells. However, this procedure cannot be done in a new project. The present work aims to show numerical procedures for estimation of the local heat transfer coefficients, at the liquid bath and metal regions, independent of previous measurements. The influence of interpolar distance, anode-ledge channel width, interanode channels width, anode width, anode slots and anode immersion depth as well the anode current density on heat transfer coefficients are investigated by numerical experiments.

### Introduction

In the aluminum reduction cells, it is necessary to have frozen bath layer on the cavity walls to contain liquid bath and liquid metal in order to protect the cell lining from this aggressive environment. Proper thickness of this layer is assured by good thermal design of the cell. Principles of cell thermal design, laid down by Haupin [1], consist of a set of thermal balance equations, which depend on heat transfer coefficients between the internal liquids and frozen ledge. Nowadays, computational power is available for high level of refinement in 3D thermal calculations [9]. Unfortunately, the behavior of heat transfer coefficients at the ledge surface seems not to be completely understood [8], particularly at the metal level.

Direct coupling between electrical, thermal and MHD processes [10] is a recent trend, which involves investment on software development. Still, the model presented in [10] does not consider some interfacial phenomena such as the presence of a bath film between ledge and metal.

The majority of the existent models use empirical heat transfer coefficients. Normally, these coefficients are determined indirectly through temperature, external cell heat flux, and ledge measurements in existing cells. In designing a new cell, no such measurements would be available.

This paper presents numerical procedures for estimation of heat transfer coefficients, based on local calculated fluid velocities and physical properties. In the bath region, a Computational Fluid Dynamics (CFD) model was built to take in to account bubble driven flow, the coefficients are obtained with classical wall function laws, which are implemented in the commercial code ANSYS CFX. In the metal region, MHD fluid flow is calculated and a special Nusselt correlation for liquid metals is adopted and, subsequently, the obtained coefficient is corrected to take into account the presence of bath film.

This modeling procedure is not independent of empirical correlations, but it relies on classical thermal boundary layer laws found in specialized heat transfer literature [6], which is applicable to a wide range of geometries.

### Bath-Ledge Heat Transfer Coefficients

It has been shown that bubble driven flow is the dominant part of the bath flow inside the channels [4, 5]. Therefore, a CFD model was developed by PCE taking into account the bubble driven flow in a quarter of cell, where the following physics is solved simultaneously:

- Fluid flow Navier-Stokes equations for bath and for  $CO_2$ ;
- Continuity equation for bath and  $CO_2$ ;
- Momentum transfer between bath and  $CO_2$ : bath is treated as continuous phase and  $CO_2$  is treated as dispersed gas phase (bubbles);
- Thermal energy transfer equation;
- K-epsilon turbulence model.

The bath thermal conductivity is an important model input. A value of  $0.8 \text{ W/mK}$  was used following the recommendation of Khokhlov et al. [3], who measured thermal conductivities of many different bath compositions.

### Application Model (Bath-Ledge Interface)

The geometry took into account the rounded anode edges, which are due to high current concentrations at beginning of anode life in the cell as shown in Figure 1. A quarter of a cell is modeled.

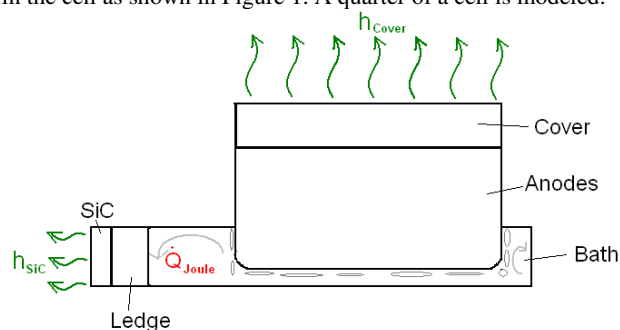


Figure 1: Schematic view of the model used to calculate bath heat transfer coefficients

Complete solid geometry details are not important in this model because heat transfer coefficients are functions of the liquids properties and fluid flow characteristics, which are the focus of the modeling.

The multiphase flow is calculated in the bath region with a continuous phase (*bath*) and a disperse phase ( $CO_2$ , with mean bubble diameter of 5 mm). The rate of  $CO_2$  generation of  $9.88 \times 10^{-4} \text{ kg/m}^2\text{s}$  at the anodes is for a cell working at 164 kA with current density of  $0.93 \text{ A/cm}^2$  and 93% CE. The modeled

geometry of the 18 anodes is the half-life size (1254 mm x 780 mm x 380 mm). The gas outflow occurs at the top of the bath domain (degassing boundary). The sidewall channels are 240 mm wide; interanode channels width is equal to 70 mm; anode to cathode distance (ACD) is 60 mm and all anodes are immersed 140 mm in the bath.

Figure 2 shows the streamlines of the bath flow for the model with the parameters described above. Figure 3 shows a top view of the bath flow behavior, and Figure 4 presents a cut view of bath bubble driven flow.

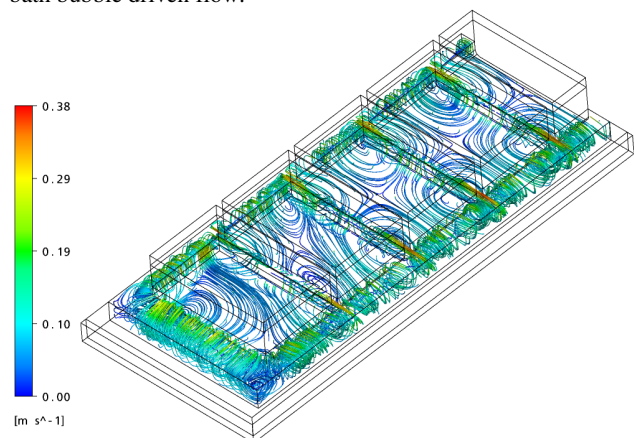


Figure 2: Bath bubble driven flow: general view

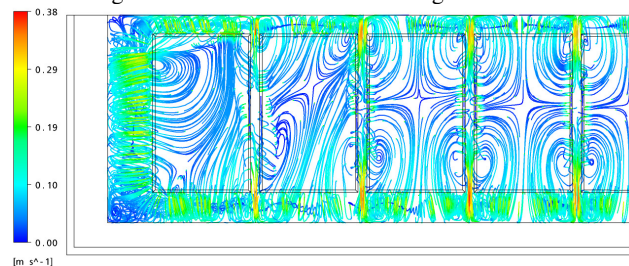


Figure 3: Bath bubble driven flow: top view

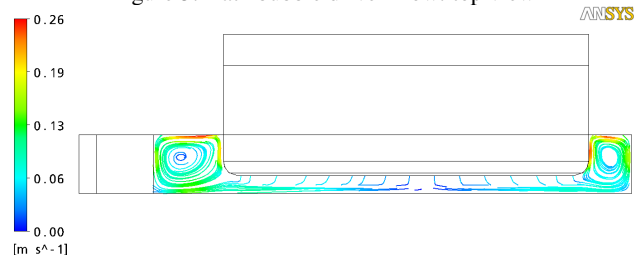


Figure 4: Bath bubble driven flow: cut view

The heat transfer equation was solved in order to calculate the wall heat transfer coefficient distribution at the bath-ledge interfaces and at bath-anode interfaces. Figure 5 shows these calculated coefficients in form of a distribution map. The thermal boundary layer is modeled using the thermal law-of-the-wall function of B.A. Kader [12], which is implemented in ANSYS CFX commercial code by the set of equations:

$$h_b = \frac{\rho c_p u^*}{T^+} \quad (1)$$

$$T^+ = Pr y^* e^{(-\Gamma)} + (2.12 \ln(y^*) + \beta) e^{(-1/\Gamma)} \quad (2)$$

$$\beta = (3.85 Pr^{1/3} - 1.3)^2 + 2.12 \ln(Pr) \quad (3)$$

$$\Gamma = \frac{0.01(Pr y^*)^4}{1 + 5 Pr^3 y^*} \quad (4)$$

where:

- $h_b$  is the heat transfer coefficient between the ledge and liquid bath;
- $cp$  the fluid heat capacity;
- $Pr$  is the fluid Prandtl number;
- $u^*$  is the dimensionless velocity near the wall relative to skin friction velocity;
- $y^*$  is the dimensionless position with respect to the boundary layer thickness.

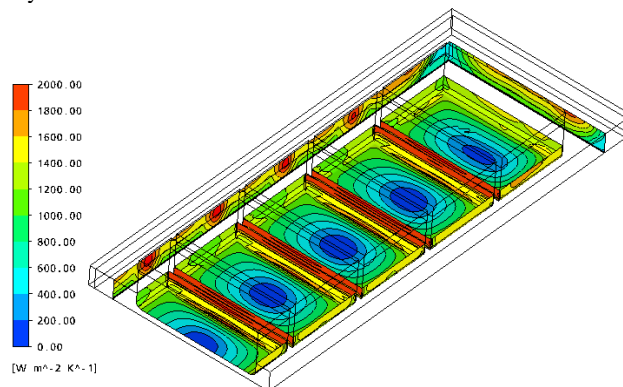


Figure 5: Wall heat transfer coefficient distribution

Fluid flow is more intense in the regions near the narrow channels between anodes, resulting in higher heat transfer coefficients in this zone. In the other hand, the region under the anodes presents a stagnation zone in its center which is responsible for low heat transfer coefficients.

The averaged wall heat transfer coefficients obtained were 1370 W/m<sup>2</sup>°C for bath-ledge and 1130 W/m<sup>2</sup>°C for bath-anode interface. These values are somewhat higher than the obtained using the correlations presented by Khokhlov et al. [3] which are around 780 W/m<sup>2</sup>°C.

#### Sensitivity Study

Based in the same specifications presented in the previous application model, the influence of some geometrical and operational parameters were studied after running sets of predefined models given in Table 1. The anode slots presence was tested too. The following sections will present and discuss the results.

Table 1: Values used in the calculations for each parameter

Sidewall Channel Width [mm]	Interanode Channels Width [mm]	Anode Immersion Depth [mm]	Anode Current Density [A/cm <sup>2</sup> ]	Anode Width [mm]	Anode Length [mm]	ACD [mm]
120	15	80	0.81	500	1050	30
180	30	110	0.85	650	1250	40
240	50	140	0.89	780	1450	50
300	70	170	0.93	850	1650	60
360	90	200	0.97			70
420	110	230	1.01			
			1.05			

### Influence of Anode-Ledge Channel Width

In the correlations presented by Solheim and Thonstad [2], the influence of the anode-ledge distance was studied experimentally. We ran our numerical model in order to confirm the behavior of heat transfer coefficients with respect to the channel width, as shown in Figure 6.

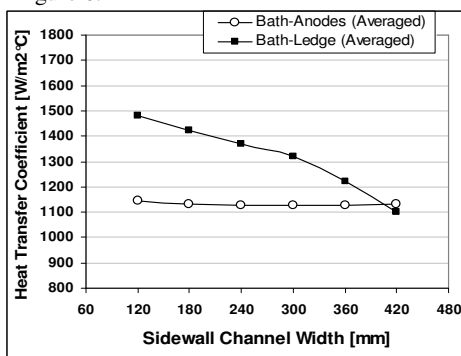


Figure 6: Averaged wall heat transfer coefficients at anodes and side ledge versus sidewall channel width.

Heat transfer coefficient at the ledge becomes smaller when increasing the side channel. This occurs because the bubble concentration is higher in a narrower channel than in a wider channel. This behavior is the same as observed experimentally [2]. At anodes, the heat transfer coefficient changes little with sidewall channel width.

### Influence of Anode Immersion Depth

The anode immersion depth is the most important factor in the heat transfer coefficients calculation. Bubbles have to travel from anode bottom surface to leave the bath at channels top due the buoyancy force. This force accelerates the bubbles inside the bath vertically. The higher the anode immersion the more space the bubbles have to accelerate and to induce the bath flow by drag force effect. Because of that, the bath flow, and as well the heat transfer coefficients, are more intensive with a higher anode immersion depth.

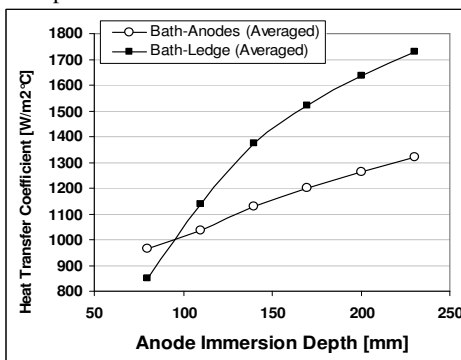


Figure 7: Averaged wall heat transfer coefficients at anodes and side ledge versus anode immersion depth.

Anode immersion depth usually varies inside a cell due to metal-bath interface shape, as the ACD is kept approximately constant under all anodes. Normally, the metal-bath interface is more elevated at the cell center, resulting in a smaller immersion in this region and a bigger immersion at the cell ends or sides, depending on cell technology. In the calculations, constant immersion was considered which can be understood as average immersion depth.

### Influence of Interanode Channels Width

The small channel between two adjacent anodes can be an important factor influencing the bubble flow behavior. A narrow channel can have difficulties to eliminate the  $CO_2$  by these channels, leading the majority of the bubbles to the side channels and the center channel. Figure 8 shows the averaged heat transfer coefficient for bath-ledge interface and bath-anode interface as a function of interanode channel width.

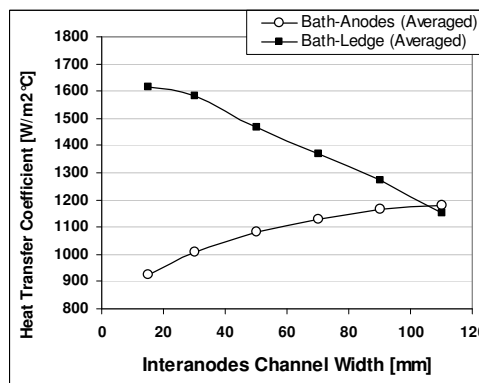


Figure 8: Averaged wall heat transfer coefficients at anodes and side ledge versus interanode channels width.

The amount of bubbles leaving the anode bottom by the interanode channels increases with channel width, reducing the amount available to go to the side channel. This explains why with wider interanode channels it increases the bath-anode and reduces the bath-ledge heat transfer coefficient.

### Influence of Anode Current Density

There is always a desire to increase line current in aluminum smelters. Considering the current increase and maintaining the same anode size, the numerical models was ran seven times in order to investigate the heat transfer coefficients behavior. The averaged results are shown in Figure 9.

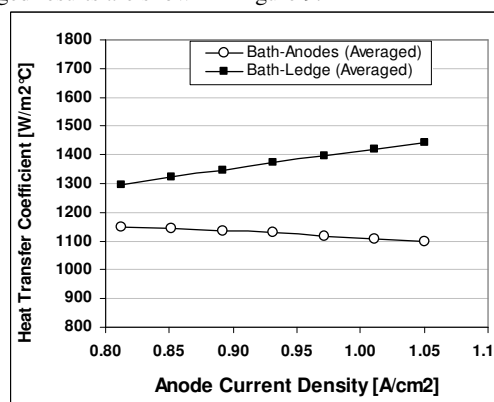


Figure 9: Averaged wall heat transfer coefficients at anodes and side ledge versus anode current density.

As expected, the heat transfer coefficient at side ledge increases with current density, as more gas is produced under the anodes, intensifying bath flow. However the anode heat transfer coefficient goes in the opposite way. This is because with higher current density, the  $CO_2$  production increases proportionally, leading to a higher bubbles total volume under the anodes. It seems that the  $CO_2$  acts as thermal insulation between bath and anode bottom decreasing the heat transfer coefficient.

### Influence of Anode Width

The numerical experiments with modifying the anode width and maintaining the same current density showed that when using wider anodes, the flow becomes more intensive at the side channels and less intensive at the interanode channels, because the  $CO_2$  flow is redirected towards the side channels. This is the explanation for the behavior of Figure 10 where the heat transfer coefficients increase at the bath-ledge interface and decrease at the bath anode interfaces with wider anodes.

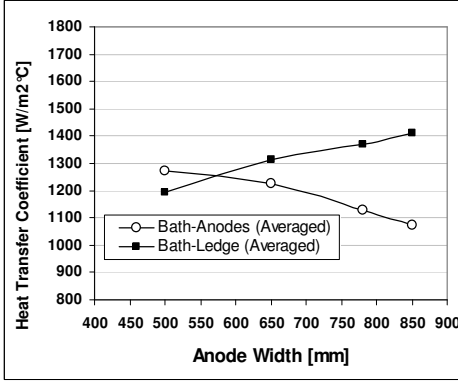


Figure 10: Averaged wall heat transfer coefficients at anodes and side ledge versus anode width.

### Influence of Anode Slots

Anode slots modify the flow pattern at the bath level, collecting the  $CO_2$  more efficiently through the slots. The bubbles travel a shorter path under the anode decreasing its influence on the global agitation. The longitudinal slots direct the streams towards the side channels (and center channel) increasing heat transfer coefficients in these regions. Transversal slots direct the flow to the interanode channels, decreasing side channels heat transfer but increasing anode-bath heat transfer. The results for different slot configurations are shown in the Figure 11.

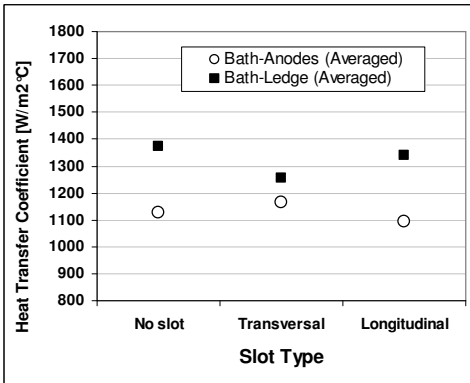


Figure 11: Averaged wall heat transfer coefficients at anodes and side ledge for different slots configuration.

### Influence of Anode Length

The same current density was maintained for four different anode lengths. The heat transfer behavior at the ledge was not modified and some influence is observed at the anode surface, decreasing with the anode length as shown in Figure 12. This result is expected because the side channel hydrodynamics was not modified. However, at the anodes, the longitudinal areas changed.

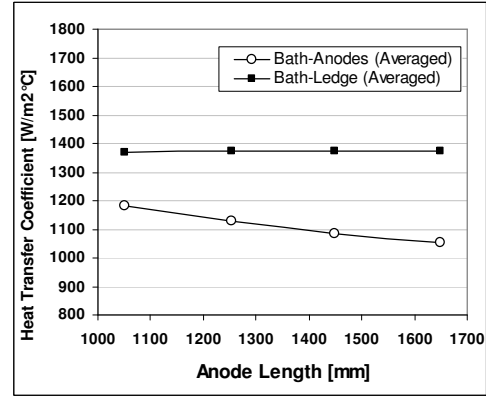


Figure 12: Averaged wall heat transfer coefficients at anodes and side ledge versus anode length.

### Influence of Anode to Cathode Distance

Bubbles formed under the anodes have to travel inside the ACD for some time until they reach the anode periphery. Squeezing the ACD causes difficulties for the bubble movement inside the bath, decreasing their velocity. The tendency of increasing heat transfer coefficient with higher ACD is shown in Figure 13, mainly at the anode surfaces.

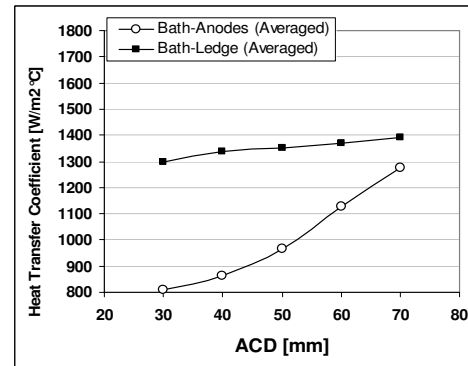


Figure 13: Averaged wall heat transfer coefficients at anodes and side ledge versus ACD.

### Metal-Ledge and Metal-Cathode Heat Transfer Coefficients

In the metal region, another approach was used. In the metal, MHD flow is dominant and no symmetry for the CFD model is possible. In this case, a Nusselt correlation [6] for liquid metals was used to obtain the coefficients, which depends on the skin shear stress ( $\tau_{wall}$ ) in the fluid near the walls, as described below.

$$\frac{h_m D_H}{k_m} = Nu_m = 4.8 + 0.0156 Re^{0.85} Pr^{0.93} \quad (5)$$

$$Re = \frac{\rho_m V^* D_H}{\mu_m} \quad (6)$$

$$V^* = \left( \frac{\tau_{wall}}{\rho_m} \right)^{0.5} \quad (7)$$

where:

- $h_m$  is the heat transfer coefficient between the ledge and liquid metal or cathode blocks and liquid metal;
- $D_H$  is the equivalent hydraulic diameter of the bulk flow;

- $k_m$  is thermal conductivity of liquid aluminum;
- $Nu_m$ , Nusselt Number for liquid aluminum flow;
- $Re$ , Reynolds Number;
- $Pr$ , Prandtl Number;
- $\rho_m^*$  density of liquid aluminum;
- $V^*$  is the wall friction velocity associated with the boundary layer;
- $\mu_m$ , viscosity of liquid aluminum;
- $\tau_{wall}$  is the wall shear stress promoted by the fluid movement.

The hydraulic diameter of the cavity is evaluated following the recommendation of W. E. Haupin [1]:

$$D_H = \frac{4H_m R_m}{2H_m + R_m} \quad (8)$$

where:

- $H_m$  is the metal height;
  - $R_m$  is the radius of rotation of molten metal;
- Thermal conductivity of liquid aluminium used in the Nusselt calculations is 100 W/m.K [11].  
The CFD model calculates the shear stress numerically and then wall heat transfer coefficient map is evaluated using the correlation (5).

#### Bath Film

Several authors [1, 7, 8] discussed the existence of a liquid bath film between liquid metal and solidified ledge. Hansen et al.[7] presented methods of evaluation of the film thickness (typical values found between 0.1 mm and 0.4 mm). As proposed by Haupin [1], metal-ledge heat transfer coefficients can be corrected adding the extra thermal resistance of the bath film:

$$h_{eff} = \frac{1}{\left(\frac{1}{h_m} + \frac{\delta}{k_b}\right)} \quad (9)$$

where:

- $h_{eff}$  is the effective heat transfer coefficient between the ledge and liquid metal including the bath film;
- $\delta$  is the bath film thickness;
- $k_b$  is thermal conductivity of liquid bath.

Bath film thickness is evaluated following the procedure proposed in [7] for the so called rigorous model:

$$\delta = 2.64 \frac{\Delta\sigma}{L(\rho_m - \rho_b) g_x} \quad (10)$$

where

- $L$  is the film length;
- $\rho_m$  is density of liquid aluminum;
- $\rho_b$  is density of liquid bath;
- $g_x$  is the acceleration of gravity component parallel to the film;
- $\sigma$  is the interfacial tension along the film, which can be related with the NaF/AlF<sub>3</sub> molar ratio along the film "r" by the relationship:

$$\Delta\sigma = -0.0875\Delta r \quad (11)$$

A value of 0.6 was used for  $\Delta r$  in all calculations.

#### Application Model (Metal-Ledge and Metal-Cathode Interface)

Figure 14 shows the calculated MHD flow at the middle of metal pad, for the Albras AP13 technology. Applying equations (5) to (11), we obtain a wall heat transfer coefficient map at the sidewall

ledge and on the cathode blocks (Figure 15). Bath film is assumed to exist only at the ledge region.

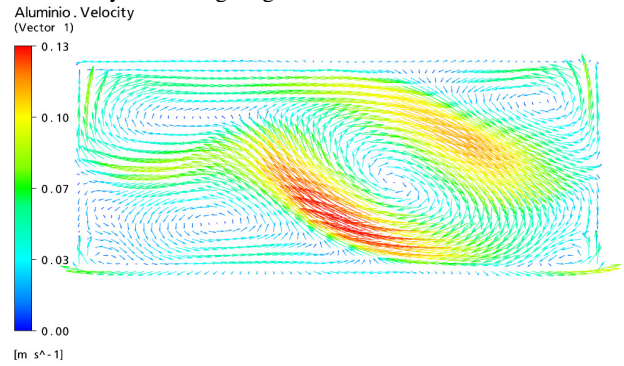


Figure 14: Metal pad velocities for Albras cell.

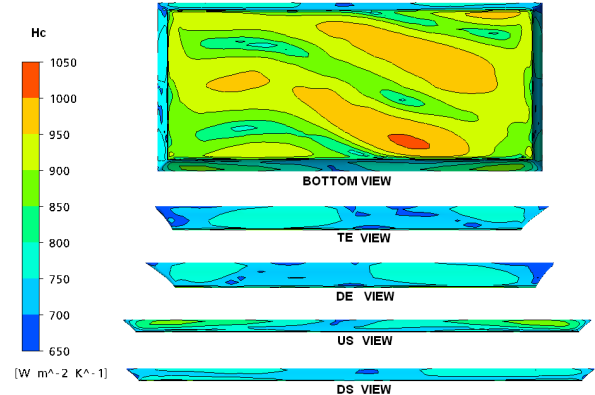


Figure 15: Wall heat transfer coefficients distribution calculated for cathode surface, sidewall ledge and endwall ledge.

Comparing Figure 14 and Figure 15, we can easily see the direct relationship between metal velocities and heat transfer coefficients. These are higher at the cathode surface, where no bath film was assumed to exist in the calculations.

#### Model Validation

The modeling procedures described in this article have been applied by the authors in several real technologies successfully. Shell heat flux measurements revealed that only when using the correct heat transfer coefficients, the corresponding heat fluxes in the thermal modelling was obtained. Figure 16 shows the comparison between measured and calculated heat fluxes for 4 different real cells.

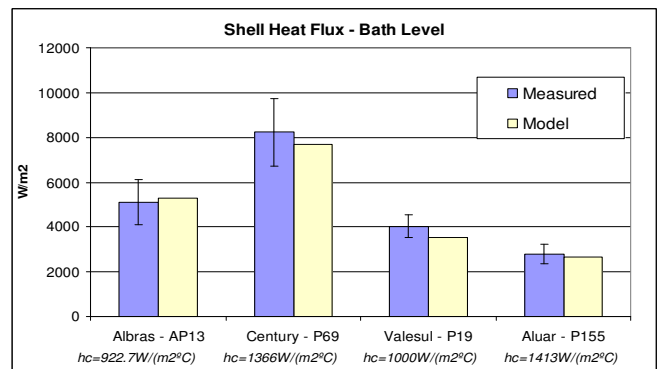


Figure 16: Measured and calculated shell heat fluxes at the bath level for different technologies

Figure 17 shows the measured ledge averaged position (and deviation) of three pots in four different positions for Aluar P155 cells using “hc” in the metal of 625 W/m<sup>2</sup>C, bath temperature of 960°C and superheat of 6°C.

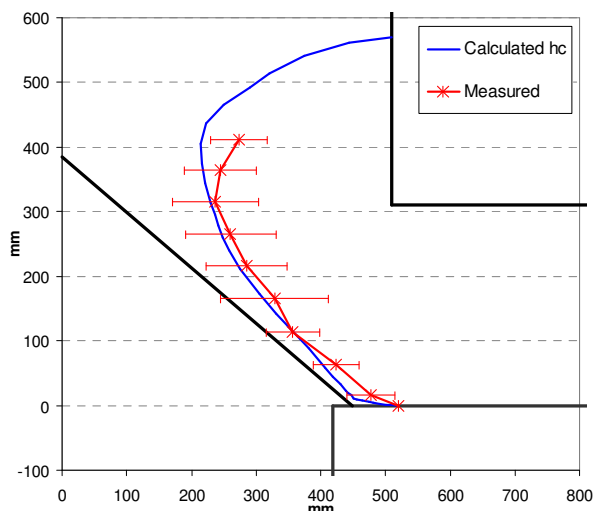


Figure 17: Measured and calculated ledge profile for Aluar-P155 cells

#### Influence of Heat Transfer Coefficient on Ledge Thickness

Three numerical model runs were made in order to show the importance of a good estimation of the heat transfer coefficients inside the cell cavity. Liquidus temperature and superheat were fixed at the values of 945°C and 9°C respectively.

In Figure 18, the green solid line represents the ledge position obtained by thermal calculation using heat transfer coefficients evaluated by the modeling procedure presented in this paper. The red (large traced) line result considers coefficients of 1000 W/m<sup>2</sup>C (metal and bath regions) and the blue (small traced) line result is calculated with 500 W/m<sup>2</sup>C (metal and bath regions).

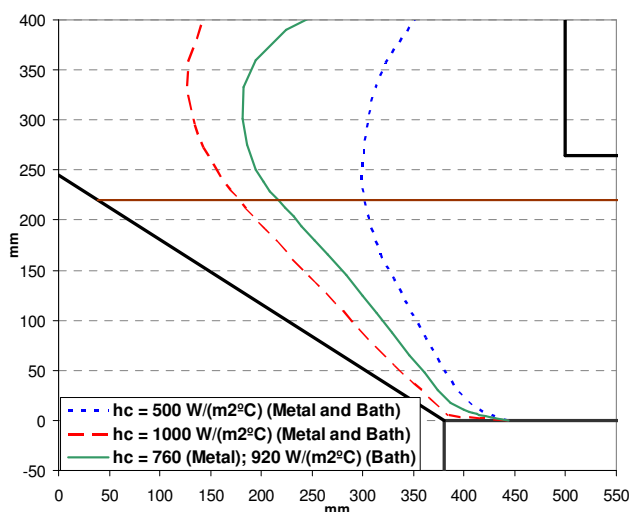


Figure 18: Ledge calculations for different values of heat transfer coefficients

#### Conclusions

A methodology for evaluation of heat transfer coefficients inside the cell was developed by combining numerical techniques and traditional heat transfer correlation formulae. Influences of geometric parameters and anode current density on the heat transfer of the cell were studied.

The results showed that the anode immersion depth is the most significant parameter, modifying the heat transfer coefficients due to the buoyancy force acting on the bubble driven flow.

Heat flux and ledge thickness model results are in agreement considering the measured variability range.

Strong dependence in the ledge shape is observed for different heat transfer coefficients. It should be noted that superheat value also needs to be correctly specified in the model, since it is the driving force of heat transfer through the solidified boundary.

#### Acknowledgement

The authors wish to thank Aluar, Albras, Century and Valesul for the permission to publish the measurements and model results.

#### References

1. W. E. Haupin, "Calculating Thickness of Containing Walls Frozen from Melt", *Light Metals*, (1971), 188-194
2. A. Solheim, J. Thonstad, "Heat Transfer Coefficients Between Bath and Side Ledge. Model Experiments", *Light Metals*, (1983), 425-435.
3. V. A. Khokhlov, E. S. Filatov, A. Solheim, J. Thonstad, "Thermal Conductivity in Cryolitic Melts- New Data and its Influence on Heat Transfer in Aluminium Cells", *Light Metals*, (1998), 501-506.
4. D. S. Severo, V. Gusberti, E. C. V. Pinto, R. R. Moura, "Modeling the Bubble Driven Flow in the Electrolyte as a Tool for Slotted Anode Design Improvement", *Light Metals*, (2007), 287-292.
5. M.A. Cooksey and W. Yang, "PIV Measurements on Physical Models of Aluminium Reduction Cells", *Light Metals*, (2006), 359-365.
6. W.M. Rohsenow; J. P. Hartnett; Y. I. Cho, *Handbook of Heat Transfer*, McGraw-Hill, 3rd Edition, Chapter 5-pg 23
7. T. Hansen, A. Solheim, K. Nisancioglu, "A Hydrodynamic Model for the Bath Film Between Metal and Side Ledge in Aluminum Cells", *Light Metals*, (1996), 351-356.
8. A. Solheim, "Towards a Proper Understanding of Sideledge Facing the Metal in Aluminum Cells? ", *Light Metals*, (2006), 439-443.
9. A. Dupuis, V. Bojarevics, "Weakly Coupled Thermo-Electric and MHD Mathematical Models of an Aluminum Electrolysis cell", *Light Metals*, (2005), 449-454.
10. Y. Safa, "Simulation Numérique Des Phénomènes Thermiques Et Magnétohydrodynamiques Dans Une Cellule De Hall-Héroult", *Docteur Thesis N°3185 - École Polytechnique Fédérale de Lausanne*, (Switzerland - 2005).
11. K.C. Mills; Recommended Values of Thermophysical Properties for Selected Commercial Alloys, *The materials Information Society- Woodhead Publishing Ltd, Cambridge-England*, pg 19-25.
12. B.A. Kader, Temperature and Concentration Profiles in Fully Turbulent Boundary Layers", *International Journal of Heat and Mass Transfer*, 24(9):1541-1544, 1981.